

# Constraints On the Diffusive Shock Acceleration From the Nonthermal X-ray Thin Shells In SN 1006 NE Rim

Ryo Yamazaki<sup>1</sup>, Tatsuo Yoshida<sup>2</sup>, Toshio Terasawa<sup>3</sup>, Aya Bamba<sup>1</sup>, and Katsuji Koyama<sup>1</sup>

<sup>1</sup> Department of Physics, Kyoto University, Kyoto 606-8502, Japan

e-mail: [yamazaki@tap.scphys.kyoto-u.ac.jp](mailto:yamazaki@tap.scphys.kyoto-u.ac.jp) , e-mail: [bamba@cr.scphys.kyoto-u.ac.jp](mailto:bamba@cr.scphys.kyoto-u.ac.jp) ,  
e-mail: [koyama@cr.scphys.kyoto-u.ac.jp](mailto:koyama@cr.scphys.kyoto-u.ac.jp)

<sup>2</sup> Faculty of Science, Ibaraki University, Mito 310-8512, Japan

e-mail: [yoshidat@mx.ibaraki.ac.jp](mailto:yoshidat@mx.ibaraki.ac.jp)

<sup>3</sup> Earth & Planetary Science, Graduate School of Science, University of Tokyo, 7-3-1 Hongo, Bunkyo-ku, 113 Tokyo, Japan

e-mail: [terasawa@eps.s.u-tokyo.ac.jp](mailto:terasawa@eps.s.u-tokyo.ac.jp)

Received date/ Accepted date

**Abstract.** Characteristic scale lengths of nonthermal X-rays from the SN 1006 NE rim, which are observed by *Chandra*, are interpreted in the context of the diffusive shock acceleration on the assumption that the observed spatial profile of nonthermal X-rays corresponds to that of accelerated electrons with energies of a few tens of TeV. To explain the observed scale lengths, we construct two simple models with a test particle approximation, where the maximum energy of accelerated electrons is determined by the age of SN 1006 (*age-limited model*) or the energy loss (*energy loss-limited model*), and constrain the magnetic field configuration and the diffusion coefficients of accelerated electrons. When the magnetic field is nearly parallel to the shock normal, the magnetic field should be in the range of 20–85  $\mu$ G and highly turbulent both in upstream and downstream, which means that the mean free path of accelerated electrons is on the order of their gyro-radius (Bohm limit). This situation can be realized both in the age-limited and energy loss-limited model. On the other hand, when the magnetic field is nearly perpendicular to the shock normal, which can exist only in the age-limited case, the magnetic field is several  $\mu$ G in the upstream and 14–20  $\mu$ G in the downstream, and the upstream magnetic field is less turbulent than the downstream.

**Key words.** Acceleration of particles – ISM : Supernova remnants – X-rays : individual : SN 1006

## 1. Introduction

Galactic cosmic rays with energies of less than  $10^{15.5}$  eV (the “knee” energy) are commonly believed to be generated by supernova remnants (SNRs). SN 1006 is one of the SNRs which is thought to be an accelerator of such high energy particles. Koyama et al. (1995) discovered synchrotron X-rays from the rims of this SNR, indicating the existence of accelerated electrons with an energy more than a few tens of TeV. The detection of TeV  $\gamma$ -rays from the northeastern (NE) rim of SN 1006 (Tanimori et al. 1998) implies further evidence for the presence of high energy particles, since TeV  $\gamma$ -rays arise from the Inverse Compton (IC) process, in which cosmic microwave background (CMB) photons are up-scattered by high energy electrons (Tanimori et al. 2001), or the hadronic process, in which  $\pi^0$  particles made by collisions between accelerated and interstellar protons decay into  $\gamma$ -ray pho-

tons (Berezhko, Ksenofontov, & Völk 2002; Aharonian & Atoyan 1999).

The mechanism for cosmic ray acceleration has also been studied for a long time and the most plausible process is a diffusive shock acceleration (DSA) (Bell 1978; Blandford & Ostriker 1978; Drury 1983; Blandford & Eicher 1987; Jones & Ellison 1991; Malkov & Drury 2001). Many authors have explained the observed properties of SN 1006 in the context of the DSA but the conclusions are different due to the arbitrary assumptions on unknown physical parameters, such as the magnetic field configuration, the diffusion coefficient, the injection rate, and the electron to proton ratio (Ellison, Berezhko, & Baring 2000; Berezhko, Ksenofontov, & Völk 2002; Völk, Berezhko, & Ksenofontov 2003; Aharonian & Atoyan 1999; Reynolds 1998; Dyer et al. 2001; Allen, Petre, & Gotthelf 2001; Achterberg, Blandford, & Reynold 1998). For example, at present the origin of TeV  $\gamma$ -rays can be explained by both leptonic and hadronic models. This comes from an in-

sufficient theoretical understanding; apart from a globally successful picture of the DSA, detailed but important processes, such as the injection or the reflection of accelerated particles that determines the above unknown quantities, are not well understood. Worse yet, previous observations in the hard X-ray band had insufficient spatial resolutions to resolve small-scale structures near the shock front, and could not strongly constrain the theoretical parameters.

Recently, Bamba et al. (2003a,b) reported on the results for not only spectral but spatial studies of thermal and non-thermal shock structure in the NE rim of SN 1006 with the excellent spatial resolution of *Chandra*. Similar results are also reported by Long et al. (2003) with *Chandra* data. Bamba et al. (2003a) estimated the scale length of thermal and non-thermal X-rays in both upstream and downstream of the shock front, which means that the direct measurement of the diffusion coefficients has become possible.

In this paper, we show that the important physical parameters for the magnetic field in the acceleration site can be constrained by the spatial distribution of observed nonthermal X-rays. § 2 summarized results of data analyses by Bamba et al. (2003a). We construct two models in § 3; one is assumed that the maximum energy of accelerated electrons are determined by the age of SNR, while the other is by the energy loss process such as synchrotron or IC cooling. Finally, § 4 is devoted to the discussion on validity of our estimation. Throughout the paper, indices “u” and “d” represent upstream and downstream, respectively.

## 2. Observed Properties of Nonthermal NE shell

In this section, we summarize the observed consequence of SN 1006, which will be used in the following sections.

We used the *Chandra* archival data of the ACIS, which has the spatial resolution of 0.5 arcsec on the aim-point, on the NE shell of SN 1006 (Observation ID = 00732) observed on July 10–11, 2000 with the targeted position at (RA, DEC) = (15<sup>h</sup>03<sup>m</sup>51<sup>s</sup>.6, −41<sup>d</sup>51<sup>m</sup>18<sup>s</sup>.8) in J2000 coordinates. Bamba et al. (2003) and Long et al. (2003) report that there are very thin filaments in the hard X-ray band image, which must be the acceleration sites of high energy electrons. Details of the observation and the analysis are found in these papers.

As shown in Fig. 2 of Bamba et al. (2003), they made profiles of six filaments and found that the upstream scale length  $w_u$  ranges between 0.01 and 0.1 pc, while the downstream scale length  $w_d$  varies from 0.06 to 0.4 pc using the exponential function with adopted distance of 2.18 kpc (Winkler et al. 2003). The mean values of  $w_u$  and  $w_d$  are 0.05 pc and 0.2 pc, respectively.

Bamba et al. (2003) also fitted the X-ray spectra for the six filaments with an *srcut* model in the XSPEC package (Reynolds 1998; Reynolds & Keohane 1999). The radio spectral index of 0.57 was adopted from the result of Allen et al. (2001). As a result, the best-fit roll-off frequency  $\nu_{\text{rolloff}} = 2.6$  (1.9–3.3)  $\times 10^{17}$  Hz was derived. The

quantity  $\nu_{\text{rolloff}}$  is written in terms of magnetic field ( $B$ ) and the maximum energy of accelerated electrons ( $E_{\text{max}}$ ) as (Reynolds & Keohane 1999)

$$\nu_{\text{rolloff}} = 5 \times 10^{17} \text{ Hz} \left( \frac{B}{10\mu\text{G}} \right) \left( \frac{E_{\text{max}}}{100\text{TeV}} \right)^2. \quad (1)$$

Since most of the nonthermal X-ray photons are observed in downstream, the synchrotron radiation is mainly due to the downstream region. Therefore, it is possible to adopt  $B$  in Eq. (1) with the downstream magnetic field  $B_d$ .

## 3. Interpretation of the Observed Width of Nonthermal X-ray Filaments

In this section, we explain the observed scale length of nonthermal X-ray filaments. Two simple models are considered in a context of DSA with a test-particle approximation. We assume that the spatial distribution of nonthermal X-rays coincides with that of the accelerated electrons to the maximum energy, while thermal X-rays trace the spatial profile of a background plasma and hence a magnetic field. For a steady state, there is no spatial structure of accelerated particles in downstream (Blandford & Ostriker 1978). However, one should consider the finite-time or energy-loss effect, which makes the spatial profile in downstream.

For simplicity, we assume magnetic fields are spatially uniform both in the upstream and downstream at least in the nonthermal X-ray emitting region. Since the fraction of magnetic pressure to the ram pressure is estimated as  $(B^2/8\pi)/(m_{\text{H}}n_{\text{u}}u_{\text{u}}^2) \sim 2 \times 10^{-5}(B/10\mu\text{G})^2$ , where we assume the number density of thermal plasma  $n \sim 1 \text{ cm}^{-3}$  and the shock velocity  $u_{\text{s}} \sim 3 \times 10^3 \text{ km s}^{-1}$ , the magnetic pressure does not affect the dynamics of SNR. We therefore can adopt the self-similar solution derived by Ratkiewicz, Axford, & Mckenzie (1994). Our assumption of spatially uniform magnetic field is a good approximation in the narrow range around the shock front.

Since the wide-band spectrum shows a break on the X-ray band, electrons accelerated near the maximum energy  $E_{\text{max}}$  contribute the nonthermal X-ray emission. The quantity  $E_{\text{max}}$  is determined by the age of SNR or by the balance of the acceleration and the energy-loss efficiencies. To discuss this, we consider three time scales; the acceleration time scale  $t_{\text{acc}}$ , the energy loss time scale  $t_{\text{loss}}$ , and the age of SN 1006  $t_{\text{age}}$ . The energy loss of high energy electrons can be neglected when  $t_{\text{acc}} < t_{\text{loss}}$ . Then,  $E_{\text{max}}$  is determined by  $t_{\text{acc}} = t_{\text{age}}$ . On the other hand,  $E_{\text{max}}$  is limited by the energy loss if  $t_{\text{acc}} = t_{\text{loss}} < t_{\text{age}}$ . We investigate these two cases separately in the following subsections.

The acceleration time is given by Drury (1983) as

$$t_{\text{acc}} = \frac{3}{u_{\text{u}} - u_{\text{d}}} \left( \frac{K_{\text{u}}}{u_{\text{u}}} + \frac{K_{\text{d}}}{u_{\text{d}}} \right), \quad (2)$$

where  $u$  and  $K$  are the velocity of bulk flow in the shock frame and the diffusion coefficients for accelerated electrons at the maximum energy, respectively. The diffusion

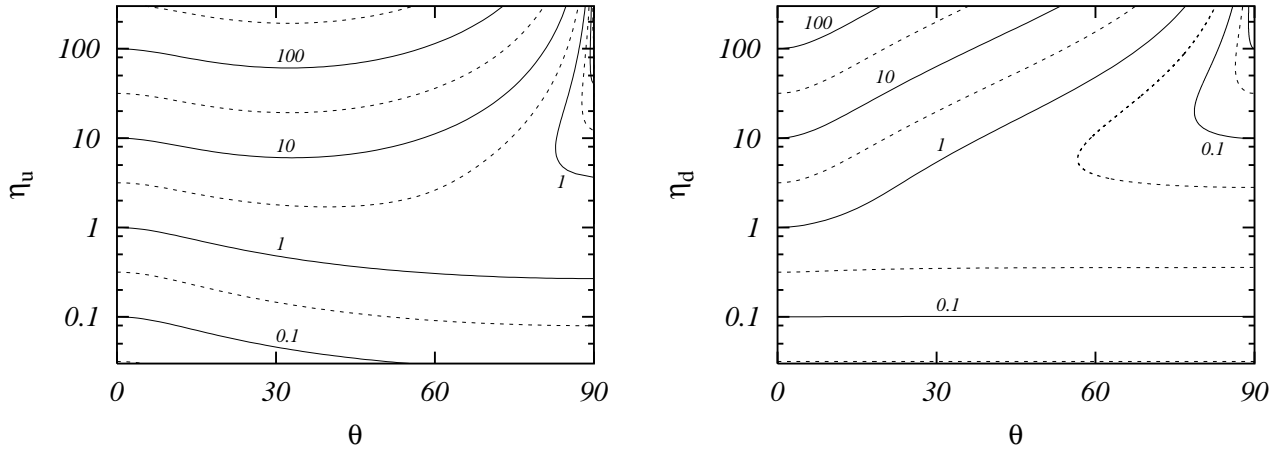


**Fig. 1.** Contour maps of the functions  $f(\eta_u, \theta)$  (left panel) and  $g(\eta_d, \theta)$  (right).

coefficients are given by quasi-linear theory (Skilling 1975; Blandford & Eichler 1987). Let the mean free path of accelerated electrons parallel to the magnetic field be a constant factor  $\eta$  times the gyro radius  $r_g = E/(eB)$  in both upstream and downstream. Then the diffusion coefficients in upstream and downstream can be written in terms of  $\eta_u$ ,  $\eta_d$ , and the angle between upstream magnetic field and the shock normal  $\theta$  (Jokipii 1987),

$$K_u = \frac{cE_{\max}}{3eB_u} \eta_u \left( \cos^2 \theta + \frac{\sin^2 \theta}{1 + \eta_u^2} \right), \quad (3)$$

$$K_d = \frac{cE_{\max}}{3eB_d} \eta_d (\cos^2 \theta + r^2 \sin^2 \theta)^{-1} \times \left( \cos^2 \theta + \frac{r^2 \sin^2 \theta}{1 + \eta_d^2} \right), \quad (4)$$

where  $r$  is the compression ratio. In this paper, since we assume that the shock is sufficiently strong and that shock structure is not affected by the cosmic-ray pressure,  $r$  should be 4 and the upstream and downstream magnetic field are related as

$$\frac{B_d}{B_u} = R(\theta) := (\cos^2 \theta + r^2 \sin^2 \theta)^{\frac{1}{2}}. \quad (5)$$

Upstream and downstream velocities are related as  $u_u = r u_d \equiv u_s$ , and throughout the paper, we adopt  $u_s = 2.89 \times 10^3 \text{ km s}^{-1}$  (Ghavamian et al. 2002). It is convenient to rewrite diffusion coefficients using Eqs. (3), (4), and (5) as

$$K_u = \frac{cE_{\max}}{3eB_d} f(\eta_u, \theta), \quad (6)$$

$$K_d = \frac{cE_{\max}}{3eB_d} g(\eta_d, \theta), \quad (7)$$

where  $f(\eta_u, \theta)$  and  $g(\eta_d, \theta)$  are given by

$$f(\eta_u, \theta) = \eta_u (\cos^2 \theta + r^2 \sin^2 \theta)^{1/2} \left( \cos^2 \theta + \frac{\sin^2 \theta}{1 + \eta_u^2} \right), \quad (8)$$

$$g(\eta_d, \theta) = \eta_d (\cos^2 \theta + r^2 \sin^2 \theta)^{-1} \left( \cos^2 \theta + \frac{r^2 \sin^2 \theta}{1 + \eta_d^2} \right). \quad (9)$$

Note that the downstream magnetic field  $B_d$  is used both in Eqs. (6) and (7). Figure 1 shows the contour plots of  $f(\eta_u, \theta)$  and  $g(\eta_d, \theta)$ . If  $\theta \gtrsim 83^\circ$ ,  $f$  can be smaller than unity in the case of  $\eta_u > 1$ . The quantity  $g$  is smaller than 0.1 for  $\eta_d > 1$  and  $\theta \gtrsim 79^\circ$ .

Next, we consider the energy loss time scale. Two processes may mainly cause the energy loss of electrons; synchrotron radiation and IC effect by cosmic microwave background photons. In the following calculations, the latter process can be neglected. Then, we can simply write

$$t_{\text{loss}} = \frac{6\pi m_e^2 c^3}{\sigma_T E B^2} = 1.25 \times 10^3 \text{ yrs} \left( \frac{E_{\max}}{100 \text{ TeV}} \right)^{-1} \left( \frac{B}{10 \mu\text{G}} \right)^{-2}. \quad (10)$$

When one compares  $t_{\text{loss}}$  with  $t_{\text{acc}}$ , the mean value of the magnetic field that accelerated electrons suffer should be adopted. We can estimate the mean magnetic field as

$$\langle B^2 \rangle = \alpha B_u^2 + (1 - \alpha) B_d^2 = \chi B_d^2, \quad (11)$$

where  $\alpha = \Delta t_u / (\Delta t_u + \Delta t_d)$  is the time fraction that accelerating electrons are in upstream. For the particles in the acceleration process, we can estimate  $\Delta t_u / \Delta t_d \sim (K_u / u_u) / (K_d / u_d) = f / (rg)$  from Eqs. (6) and (7). Then, we obtain  $\chi = (R^{-2} f + rg) / (f + rg)$ , which ranges between 0 and 1, where  $R$  is defined in Eq. (5).

### 3.1. Age-Limited Case

First, we investigate the case in which the acceleration time is nearly equal to the age of SN 1006  $t_{\text{acc}} \sim t_{\text{age}}$ . This condition implies that the observed nonthermal X-rays are emitted by electrons that have been accelerated up to now.

The particles in the diffusive shock acceleration process are transported to the upstream by the diffusion, and are advected to the downstream. The diffusion and advection time scales to move a scale-length  $w$  are  $t_{\text{adv}} = w/u$  and  $t_{\text{dif}} = w^2/K$ . In the upstream, the accelerated particles can reach up to the place at which the advection

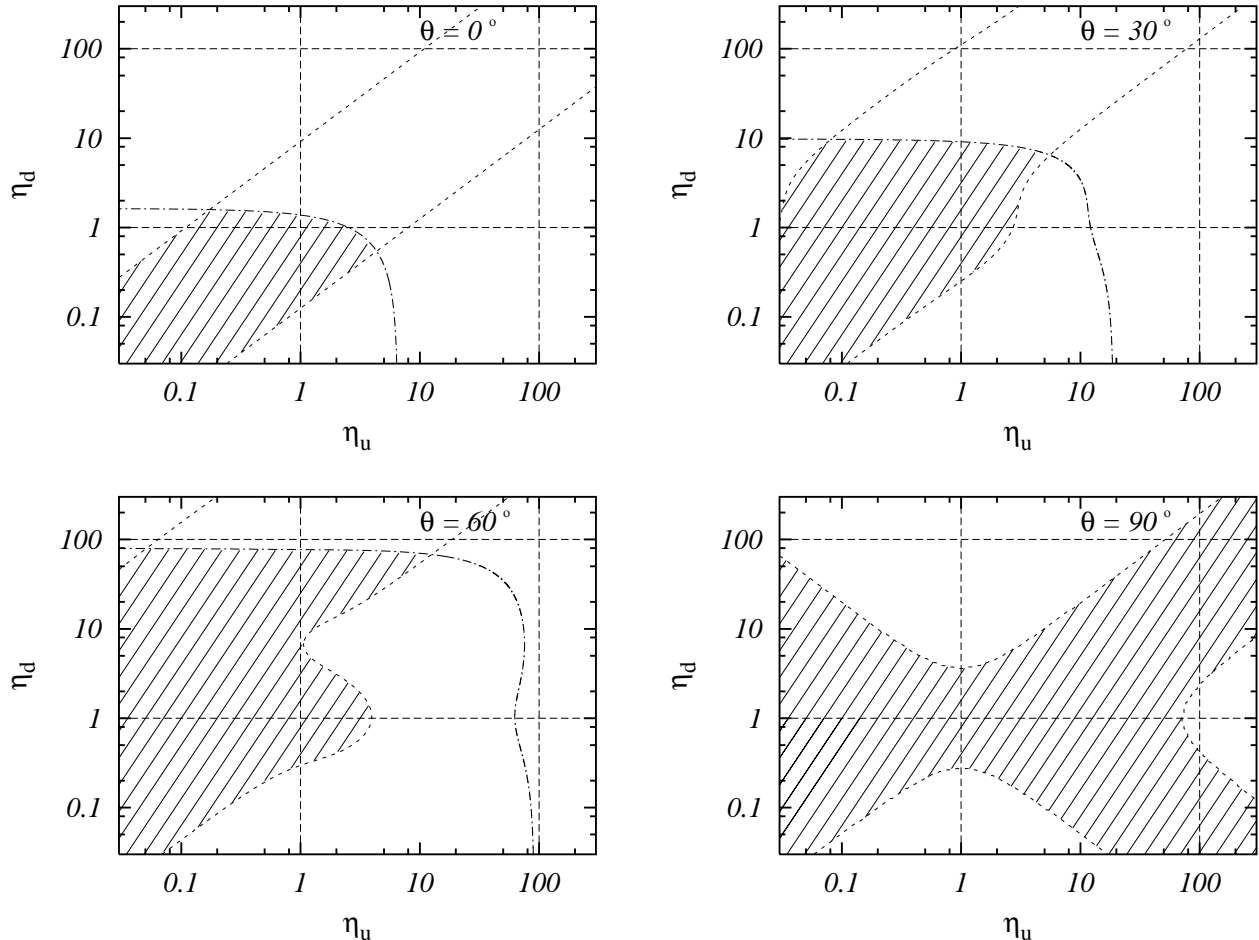


**Fig. 2.** Points in the shaded regions surrounded by dotted and dot-dashed lines satisfy Eqs. (1), (5), (12), and (13) for fixed  $\theta$  in the age-limited case. Dotted lines represent Eq. (A.1) with  $w_d/w_u = 0.6$  or 40, while dot-dashed lines Eq. (A.4) with  $\nu_{\text{rolloff}} = 1.9 \times 10^{17}$  Hz, the upper to which is forbidden since  $t_{\text{acc}} > t_{\text{loss}}$ .

is balanced with the diffusion, i.e.  $t_{\text{adv}} = t_{\text{dif}}$ . Therefore, the observed upstream-width of nonthermal X-rays can be written as

$$w_u = \frac{K_u}{u_u} = \frac{cE_{\text{max}}}{3eB_d u_s} f(\eta_u, \theta). \quad (12)$$

In the downstream, if the particles are advected too far from the shock front, they cannot return back to the upstream to get further energy. Therefore, the particles being accelerated should stay in the region where  $t_{\text{dif}}$  is smaller than  $t_{\text{adv}}$ . Thus, we obtain the same equation as upstream,

$$w_d = \frac{K_d}{u_d} = \frac{cE_{\text{max}}}{3eB_d u_s} r g(\eta_d, \theta). \quad (13)$$

Then, Eq. (2) becomes

$$t_{\text{acc}} = \frac{3r}{r-1} \frac{w_u + w_d}{u_s} \sim 3.4 \times 10^2 \text{ yrs} \left( \frac{w_u + w_d}{0.25 \text{ pc}} \right). \quad (14)$$

Since  $t_{\text{acc}}$  is comparable to the age of the SN 1006, our assumption  $t_{\text{acc}} \sim t_{\text{age}}$  is justified. Eliminating  $E_{\text{max}}$  with Eq. (1), we can rewrite (12) and (13) as

$$w_u = 0.27 \text{ pc} \left( \frac{\nu_{\text{rolloff}}}{2.6 \times 10^{17} \text{ Hz}} \right)^{\frac{1}{2}} \left( \frac{B_d}{10 \mu\text{G}} \right)^{-\frac{3}{2}} f(\eta_u, \theta), \quad (15)$$

$$w_d = 1.1 \text{ pc} \left( \frac{\nu_{\text{rolloff}}}{2.6 \times 10^{17} \text{ Hz}} \right)^{\frac{1}{2}} \left( \frac{B_d}{10 \mu\text{G}} \right)^{-\frac{3}{2}} g(\eta_d, \theta), \quad (16)$$

respectively.

Let us take  $w_u \sim 0.05$  pc,  $w_d \sim 0.2$  pc, and  $\nu_{\text{rolloff}} \sim 2.6 \times 10^{17}$  Hz as typical observed quantities (Bamba et al. 2003a). Then, Eqs. (15) and (16) give  $B_d \sim 30 f^{2/3} \mu\text{G} \sim 30 g^{2/3} \mu\text{G}$ . In the case of  $\theta \sim 0^\circ$ , the value of  $B_d$  can be determined as follows. We see that since  $\eta_u \geq 1$ ,  $f$  should be greater than  $\sim 1$ , i.e.  $B_d \gtrsim 30 \mu\text{G}$ . Independently of this, the condition  $t_{\text{acc}} \lesssim t_{\text{loss}}$  gives the upper limit of  $B_d$  as  $B_d \lesssim 30 \mu\text{G}$  (see Eq. [A.5]). Therefore, we obtain  $B_d \sim 30 \mu\text{G}$ . This argument has been done in Bamba et al. (2003a). On the other hand, as we have mentioned before, cases of  $f \lesssim 1$  can be realized if  $\theta \gtrsim 80^\circ$ , i.e. the magnetic field is nearly perpendicular to the shock normal. Then  $B_d$  may be smaller than  $\sim 30 \mu\text{G}$ .

Let us vary observed quantities  $w_u$ ,  $w_d$ , and  $\nu_{\text{rolloff}}$  in the range of the observed errors (at 90% confidence level). We have six unknown parameters  $E_{\text{max}}$ ,  $B_u$ ,  $B_d$ ,  $\eta_u$ ,  $\eta_d$ , and  $\theta$ . Conditions (1), (5), (12), (13), and  $t_{\text{acc}} \lesssim t_{\text{loss}}$  are used to relate these quantities. Details are summarized in § A. Figure 2 shows allowed regions of  $\eta_u$  or  $\eta_d$  for fixed

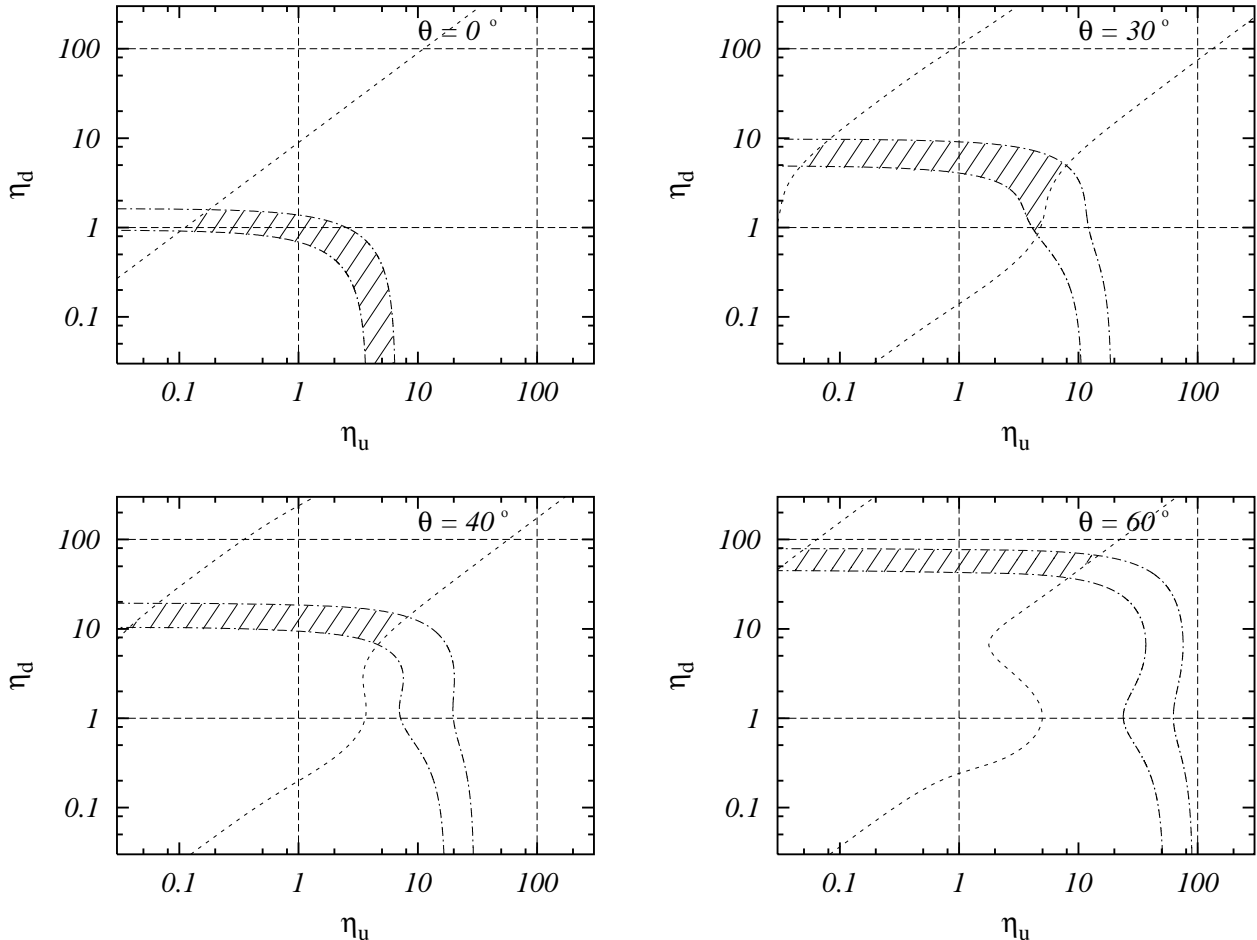


**Fig. 3.** Points in the shaded regions surrounded by dotted and dot-dashed lines satisfy Eqs. (1), (5), (17), (18), (19), and  $t_{\text{loss}} < t_{\text{age}}$  for fixed  $\theta$  in the energy loss-limited case. Dotted lines represent Eq. (A.14) with  $w_d/w_u = 0.6$  or  $40$ , while dot-dashed lines Eq. (A.13) with  $\nu_{\text{rolloff}} = 1.9 \times 10^{17}$  or  $3.3 \times 10^{17}$  Hz.

$\theta$ . When we take  $\theta = 0^\circ$ , the case of  $\eta_u = \eta_d = 1$  (Bohm limit in both upstream and downstream) is marginally acceptable, since  $\eta$  should satisfy  $1 \leq \eta \lesssim c/u_s \sim 10^2$  (Jokipii 1987). Then the magnetic field has values of  $B_u = B_d = 20\text{--}78 \mu\text{G}$ . The equation (A.5) shows that the maximum value of magnetic fields is achieved when observed quantities  $\nu_{\text{rolloff}}$ ,  $w_u$ , and  $w_d$  have the minimum values. On the other hand, when  $\theta \gtrsim 85^\circ$ , small magnetic fields are possible. If we choose  $w_u = 0.1 \text{ pc}$ ,  $w_d = 0.3 \text{ pc}$ , and  $\nu_{\text{rolloff}} = 2 \times 10^{17} \text{ Hz}$ , then  $\eta_u \sim 10$  and  $\eta_d \sim 1$ , the magnetic fields are  $B_d \sim 4B_u \sim 14\text{--}20 \mu\text{G}$ . This result has been suggested by Bamba et al. (2003a).

The left panel of Fig. 4 represents the allowed region of  $E_{\text{max}}$  and  $B_d$  (see Eqs. [A.6] and [A.7]). The solid lines describe Eq. (1) with  $\nu_{\text{rolloff}} = (1.9\text{--}3.3) \times 10^{17} \text{ Hz}$ , while the dashed lines a boundary of the region in which a gyro-radius of accelerated electrons in the downstream  $r_g = E_{\text{max}}/(eB_d) \propto g^{-1}w_d$ . In order to satisfy  $1 \leq \eta \leq 10^2$  and all of the other conditions, the quantity  $g^{-1}(w_d/\text{pc})$  should range between  $0.09$  and  $27$ .

### 3.2. Energy Loss-Limited Case

If the maximum energy of accelerated electrons  $E_{\text{max}}$  is determined by

$$t_{\text{acc}} = t_{\text{loss}}, \quad (17)$$

the motion of accelerated particles toward the upstream might be obstructed by the energy loss effect as well as the advection. Let us consider in the upstream, the energy loss time scale  $t_{\text{cool}}^1$  in addition to the advection time scale  $t_{\text{adv}} = w_u/u_u$  and the diffusion time scale  $t_{\text{dif}} = w_u^2/K_u$ . If  $t_{\text{dif}} = t_{\text{adv}} < t_{\text{cool}}$ , the observed width of nonthermal X-rays in the upstream is given by  $w_u = K_u/u_u$  as well as the age-limited case, while in the case of  $t_{\text{dif}} = t_{\text{cool}} < t_{\text{adv}}$ ,  $w_u$  is given by  $w_u = (K_u t_{\text{cool}})^{\frac{1}{2}}$ . Therefore, we can write

$$w_u = \min\{K_u/u_u, (K_u t_{\text{cool}})^{\frac{1}{2}}\}. \quad (18)$$

On the other hand, the observed scale length of non-thermal X-ray filaments in the downstream  $w_d$  is determined by the cooling time scale as

$$w_d = \max\{u_d t_{\text{cool}}, (K_d t_{\text{cool}})^{\frac{1}{2}}\}. \quad (19)$$

<sup>1</sup> To avoid the confusion, here we use the notation “ $t_{\text{cool}}$ ” which is compared with  $t_{\text{adv}}$  or  $t_{\text{dif}}$ , in order to distinguish “ $t_{\text{loss}}$ ” used when one compares with  $t_{\text{acc}}$  or  $t_{\text{age}}$ .

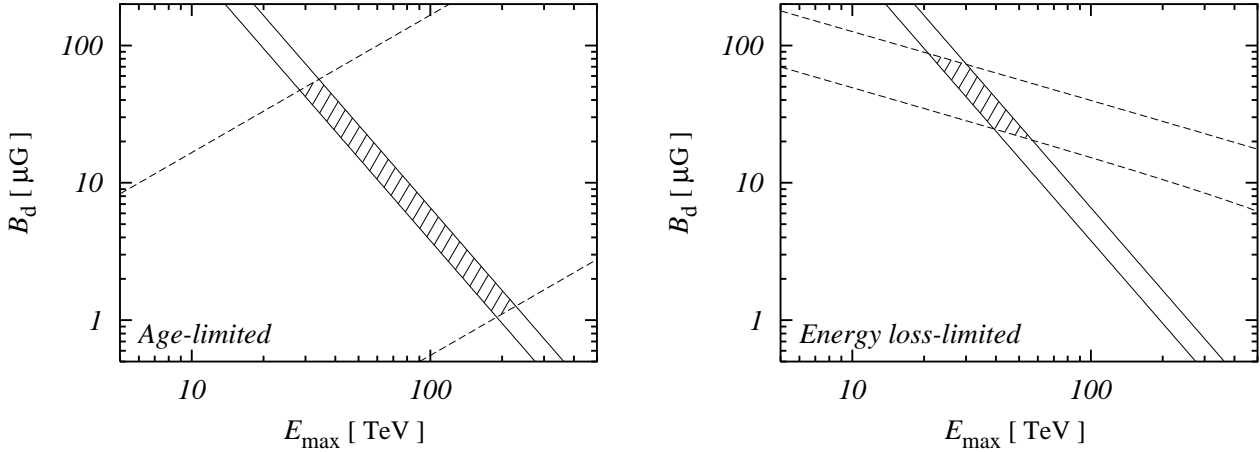


**Fig. 4.** The shaded areas indicate the most likely values of magnetic fields just behind the shock front  $B_d$  and the maximum energy of shock-accelerated electrons  $E_{\max}$ . The left panel is for the age-limited case, while the right the energy loss-limited model. These areas are formed by the two solid lines for a roll-off energy of  $\nu_{\text{rolloff}} = (1.9\text{--}3.3) \times 10^{17}$  Hz, and the two dashed lines from the observed width of nonthermal X-rays; in the age-limited case, a gyro-radius of accelerated electrons in the downstream should be  $r_g = E_{\max}/(eB_d) = (0.065\text{--}20) \times 10^{-2}$  pc, while in the energy loss-limited case, cooling time of accelerated electrons should be  $t_{\text{cool}} = w_d/u_d = (0.81\text{--}5.4) \times 10^2$  yrs.

We can now use five equations (1), (5), (17), (18), and (19) for six unknown parameters  $E_{\max}$ ,  $B_u$ ,  $B_d$ ,  $\eta_u$ ,  $\eta_d$ , and  $\theta$ , and solve these equations with fixed  $\theta$  under the condition of  $t_{\text{loss}} < t_{\text{age}}$ . We summarize a detailed calculation procedure in § A.

Figure 3 shows the results for individual  $\theta$ . We consider, as well as the age-limited case, the errors associated with the analysis of Bamba et al. (2003a). When  $\theta = 0^\circ$ , the case of  $\eta_u = \eta_d = 1$  is again acceptable. Then, the magnetic field is in the range of  $B_u = B_d = 23\text{--}85$  μG. If  $\theta \lesssim 30^\circ$ , the downstream magnetic field can be in the Bohm limit  $\eta_d = 1$ , then  $\eta_u \sim 1\text{--}8$  and  $B_d \sim 23\text{--}85$  μG. However, if  $\theta$  is larger than  $\sim 35^\circ$ , then  $\eta_d \gtrsim 10$  and  $\eta_u \lesssim 10$ . This implies that the upstream magnetic field is more turbulent than the downstream, which seems to be unrealistic.

Indeed, as shown in § A.2, scale lengths are given by  $w_u = K_u/u_u$  and  $w_d = u_d t_{\text{cool}}$ . Then,  $E_{\max}$  and  $B_d$  are given by Eqs. (A.10) and (A.11), respectively. The right panel of Fig. 4 represents the allowed region of  $E_{\max}$  and  $B_d$  when  $w_d = 0.06\text{--}0.4$  pc and  $\nu_{\text{rolloff}} = (1.9\text{--}3.3) \times 10^{17}$  Hz. All the points in the region satisfy other conditions. Vink & Laming (2003) discussed similar arguments for Cas A.

## 4. Discussion

We have argued the limitations on the model of DSA from the recently observed scale length of nonthermal X-ray emitting region of NE shell of SN 1006 based on the assumption that the observed spatial structure of nonthermal X-ray filaments reflects that of accelerated electrons to the maximum energy. A test particle approximation has been adopted, where the back reactions of accelerated particles are neglected, although one might have to consider corrections due to nonlinear effects in order to ex-

plain the wide-band spectrum from radio to TeV  $\gamma$ -rays. Two models have been discussed; age-limited and energy loss-limited models. Note that in each model, the value and configuration of a magnetic field in the acceleration site can be discussed using only the spatial distribution of the synchrotron X-rays, which are emitted by accelerated electrons with energy several tens of TeV, and the roll-off frequency, which is derived by the fitting of the wide band spectrum from the radio to X-rays.

When a magnetic field is nearly parallel to the shock normal,  $\eta_u$  and  $\eta_d$  should be nearly unity, which means that the magnetic field is highly turbulent (near the Bohm limit), and the magnetic field is in the range of 20–85 μG. Relatively strong parallel magnetic fields are considered by several authors (Berezhko et al. 2002; Ellison et al. 2000). Derived value of the magnetic field seems to be higher than the usual interstellar value of a few micro Gauss. However, the mechanism pointed by Lucek & Bell (2000) may be able to amplify the magnetic field. These situation can be realized both in the age-limited and energy loss-limited model.

When the magnetic field is nearly perpendicular to the shock normal, relatively small values of  $B_d = 4B_u = 14\text{--}20$  μG are allowed, which can exist only in the age-limited model. This value is consistent with the interstellar magnetic field and assumed value in Bamba et al. (2003a) or other papers (Allen et al. 2001; Reynolds 1998) but slightly larger than that derived by CANGAROO observation (Tanimori et al. 1998, 2001), which assumes TeV  $\gamma$ -rays are emitted by the IC process. This discrepancy may be solved if the filaments 1–6 are not the main sites of TeV  $\gamma$ -rays generated by the leptonic process. The observed flux of TeV  $\gamma$ -rays which are up-scattered CMB photons by synchrotron emitting electrons is written as

$$\mathcal{F}_{\text{IC}} = 2.5 \times 10^{-2} \left( \frac{B_d}{20 \text{ μG}} \right)^{-2} \mathcal{F}_{\text{synch}}, \quad (20)$$

where  $\mathcal{F}_{\text{synch}}$  is the observed flux of synchrotron X-rays and estimated as  $1.8 \times 10^{-12}$  ergs  $\text{s}^{-1}$   $\text{cm}^{-2}$  in the 0.5–10.0 keV band by Bamba et al. (2003a). Then, the contribution of the IC  $\gamma$ -rays generated in the filaments 1–6 is only  $\sim 0.5\%$  of the whole flux coming from SN 1006. This shows that the IC  $\gamma$ -ray emitting sites have smaller magnetic field, hence radiate less synchrotron X-rays than in the filaments 1–6. Or the TeV  $\gamma$ -rays might be emitted by the hadronic process. In fact the most plausible position of the  $\gamma$ -ray emission determined by CANGAROO is located north (and outside) of the filament 1 (Tanimori et al. 1998, 2001). However, the region where the significance is higher than half the maximum value extends over  $\sim 0.2^\circ$ , which is almost the same as the standard deviation of the point-spread function of the CANGAROO telescope. We need stereoscopic observations of TeV gamma-ray emissions by imaging atmospheric Cherenkov telescopes (for example, CANGAROO-III, HEGRA, and H.E.S.S.) to establish the position and extent of the emission region.

We briefly discuss how our results may change if the test particle approximation is dropped. Although we should consider the spatial structure modified, for example, in the upstream precursor region, we simply argue the cases of  $r > 4$  that are thought to be caused by nonlinear effects. Indeed, Berezhko, Ksenofontov, & Völk (2002) showed that the present value of total compression ratio is about 6. In the age-limited case, we observe that the inferred magnitude of the upstream magnetic field becomes smaller than that of the  $r = 4$  case as  $r$  is made larger (up to 7). However, the overall shapes and total areas of the allowed regions are changed only slightly for any case of  $\theta$ . Thus the nonlinear effect would not be essential. On the other hand, in the energy loss-limited case, the allowed region in the  $\eta_u$ – $\eta_d$  plane becomes narrow and only the cases of  $\theta = 0^\circ$ – $10^\circ$  can be exist for  $4 < r \lesssim 6$  while no allowed region for  $r \sim 7$  case. This comes from the fact that another restriction, Eq. (A.24), emerges. The larger  $r$ , the stronger the constraint because of the less efficient advection for fixed shock velocity  $u_s$ . Furthermore, it can be shown that there exists no case in which  $w_d$  is given by  $(K_d t_{\text{cool}})^{\frac{1}{2}}$ , since the condition  $t_{\text{acc}} = t_{\text{cool}}$  is incompatible with the condition  $w_d t_{\text{cool}} < (K_d t_{\text{cool}})^{\frac{1}{2}}$  in the parameter range of our interest.

It is important to determine the magnetic field configurations in order to discuss the acceleration and/or injection efficiency. In this paper, using the spatial distribution of nonthermal X-rays, we have shown that roughly two cases can exist; high and parallel, and low and perpendicular magnetic field. In the latter case, the back reaction of accelerated particles is small and thus a test-particle treatment is a good approximation. The magnetic field amplification process pointed by Lucek & Bell (2000) does not work well. While in the former case, nonlinear effects are so efficient that the magnetic field can be large. The difference between these cases probably comes from the fact that the (proton) injection rate depends strongly on the shock obliquity and diminishes as  $\theta$  increases (Völk,

Berezhko, & Ksenofontov 2003). In addition to our result, radio polarization data with high spatial resolution may become further informations about the magnetic field configuration.

In this paper, we have adopted the plane shock approximation. For further details, it might be important to consider the curvature effect as discussed in Berezhko, Ksenofontov, & Völk (2003) in order to produce more realistic scenario.

*Acknowledgements.* Our particular thanks are due to T. Nakamura, M. Hoshino, and T. Tanimori for their fruitful discussions and comments. R.Y. and A.B. are supported by JSPS Research Fellowship for Young Scientists. This work is supported by a Grant-in-Aid for Scientific Research, No. 14340066 from the Ministry of Educations, Culture, Sports, Science, and Technology of Japan, and also supported by a Grant-in-Aid for the 21st Century COE “Center for Diversity and Universality in Physics”.

## Appendix A: Detailed calculations

We summarize a procedure of practical calculations of  $\eta_u$  and  $\eta_d$  from observed quantities. Once  $(f, g)$  is given for fixed  $\theta$ , the allowed region of  $(\eta_u, \eta_d)$  is derived by Eqs. (8) and (9). Relations of  $f$  and  $g$  in age-limited case and energy loss-limited case are different from each other.

### A.1. Age-limited case

One can derive from Eqs. (12) and (13)

$$\frac{g}{f} = r^{-1} \frac{w_d}{w_u} . \quad (\text{A.1})$$

The condition  $t_{\text{acc}} \lesssim t_{\text{loss}}$  gives the additional inequalities. Substituting Eqs. (6) and (7) into Eq. (2), we derive

$$t_{\text{acc}} = 4\phi(f + rg) \frac{cE_{\text{max}}}{3eB_d u_s^2} , \quad (\text{A.2})$$

where  $\phi = \phi(r) = (3/4)r/(r - 1)$ . Energy loss timescale that should be compared with  $t_{\text{acc}}$  is given by

$$t_{\text{loss}} = \frac{6\pi m_e c^3}{\sigma_T E_{\text{max}} B_d^2} \frac{f + rg}{R^{-2} f + rg} . \quad (\text{A.3})$$

Using Eq. (1), we can eliminate  $E_{\text{max}}$  and  $B_d$ , and obtain

$$R(\theta)^{-2} f + rg \lesssim 4.8 \phi^{-1} \left( \frac{\nu_{\text{rolloff}}}{2.6 \times 10^{17} \text{ Hz}} \right)^{-1} \times \left( \frac{u_s}{2.89 \times 10^8 \text{ cm s}^{-1}} \right)^2 . \quad (\text{A.4})$$

The quantities  $f$  and  $g$  should satisfy Eqs. (A.1) and (A.4).

The condition  $t_{\text{acc}} \lesssim t_{\text{loss}}$  gives also the upper limit of  $B_d$ . In the age limited case, one can derive  $\chi = (R^{-2} w_u + w_d)/(w_u + w_d)$ . Then using Eqs. (10) and (14), we derive

$$B_d \lesssim 30 \mu\text{G} \phi^{-2/3} \left( \frac{\nu_{\text{rolloff}}}{2.6 \times 10^{17} \text{ Hz}} \right)^{-1/3} \times \left( \frac{w_u R^{-2}(\theta) + w_d}{0.25 \text{ pc}} \right)^{-2/3} \left( \frac{u_s}{2.89 \times 10^8 \text{ cm s}^{-1}} \right)^{2/3} , \quad (\text{A.5})$$

where we eliminate  $E_{\max}$  with Eq. (1).

Additionally, using Eqs. (1) and (13), one can show  $E_{\max}$  and  $B_d$  can be expressed in terms of  $g$  as

$$E_{\max} = 41 \text{ TeV} \left( \frac{r}{4} \right)^{-1/3} \left( \frac{\nu_{\text{rolloff}}}{2.6 \times 10^{17} \text{ Hz}} \right)^{1/3} \times \left( \frac{g^{-1} w_d}{0.2 \text{ pc}} \right)^{1/3} \left( \frac{u_s}{2.89 \times 10^8 \text{ cm s}^{-1}} \right)^{1/3}, \quad (\text{A.6})$$

$$B_d = 31 \mu\text{G} \left( \frac{r}{4} \right)^{2/3} \left( \frac{\nu_{\text{rolloff}}}{2.6 \times 10^{17} \text{ Hz}} \right)^{1/3} \times \left( \frac{g^{-1} w_d}{0.2 \text{ pc}} \right)^{-2/3} \left( \frac{u_s}{2.89 \times 10^8 \text{ cm s}^{-1}} \right)^{-2/3}, \quad (\text{A.7})$$

respectively.

## A.2. Energy loss-limited case

For our parameters we consider,  $w_u$  and  $w_d$  are given by

$$w_u = K_u / u_s, \quad (\text{A.8})$$

$$w_d = u_d t_{\text{cool}}. \quad (\text{A.9})$$

We can calculate  $E_{\max}$  and  $B_d$  from Eqs. (1) and (A.9) as

$$E_{\max} = 39 \text{ TeV} \left( \frac{r}{4} \right)^{1/3} \left( \frac{\nu_{\text{rolloff}}}{2.6 \times 10^{17} \text{ Hz}} \right)^{2/3} \times \left( \frac{w_d}{0.2 \text{ pc}} \right)^{1/3} \left( \frac{u_s}{2.89 \times 10^8 \text{ cm s}^{-1}} \right)^{-1/3}, \quad (\text{A.10})$$

$$B_d = 35 \mu\text{G} \left( \frac{r}{4} \right)^{-2/3} \left( \frac{\nu_{\text{rolloff}}}{2.6 \times 10^{17} \text{ Hz}} \right)^{-1/3} \times \left( \frac{w_d}{0.2 \text{ pc}} \right)^{-2/3} \left( \frac{u_s}{2.89 \times 10^8 \text{ cm s}^{-1}} \right)^{2/3}. \quad (\text{A.11})$$

Then, from Eqs. (6) and (A.8), we derive

$$f = 4.8 \frac{w_u}{w_d} \left( \frac{r}{4} \right)^{-1} \left( \frac{\nu_{\text{rolloff}}}{2.6 \times 10^{17} \text{ Hz}} \right)^{-1} \times \left( \frac{u_s}{2.89 \times 10^8 \text{ cm s}^{-1}} \right)^2. \quad (\text{A.12})$$

The condition  $t_{\text{acc}} = t_{\text{loss}}$  gives

$$R(\theta)^{-2} f + rg = 4.8 \phi^{-1} \left( \frac{\nu_{\text{rolloff}}}{2.6 \times 10^{17} \text{ Hz}} \right)^{-1} \times \left( \frac{u_s}{2.89 \times 10^8 \text{ cm s}^{-1}} \right)^2. \quad (\text{A.13})$$

Eliminating  $\nu_{\text{rolloff}}$  from Eqs (A.12) and (A.13), we derive

$$\frac{g}{f} = \frac{1}{4} \left[ \phi^{-1} \frac{w_d}{w_u} - \left( \frac{r}{4} \right)^{-1} R(\theta)^{-2} \right]. \quad (\text{A.14})$$

Equations (A.13) and (A.14) determine  $(f, g)$ .

We can show that the condition  $t_{\text{loss}} < t_{\text{age}}$  is always satisfied. Substituting Eqs. (A.10) and (A.11) into Eq. (A.3), we obtain

$$t_{\text{loss}} = 2.7 \times 10^2 \text{ yrs} \left( \frac{r}{4} \right) \left( \frac{w_d}{0.2 \text{ pc}} \right) \times \left( \frac{u_s}{2.89 \times 10^8 \text{ cm s}^{-1}} \right)^{-1} \frac{f + rg}{R^{-2} f + rg}. \quad (\text{A.15})$$

Then,  $t_{\text{loss}} < t_{\text{age}}$  reduces

$$\frac{1 + rg/f}{R^{-2} + rg/f} < 3.7 \left( \frac{r}{4} \right)^{-1} \left( \frac{w_d}{0.2 \text{ pc}} \right)^{-1} \times \left( \frac{u_s}{2.89 \times 10^8 \text{ cm s}^{-1}} \right) \left( \frac{t_{\text{age}}}{1000 \text{ yrs}} \right). \quad (\text{A.16})$$

Using Eq. (A.14), we rewrite the left hand side of Eq. (A.16) as

$$\frac{1 + rg/f}{R^{-2} + rg/f} = 1 + (1 - R(\theta)^{-2}) \phi \left( \frac{r}{4} \right)^{-1} \frac{w_u}{w_d}. \quad (\text{A.17})$$

Substituting Eq. (A.17) into Eq. (A.16), we derive

$$w_d + (1 - R(\theta)^{-2}) \phi \left( \frac{r}{4} \right)^{-1} w_u < 0.74 \text{ pc} \left( \frac{r}{4} \right)^{-1} \left( \frac{u_s}{2.89 \times 10^8 \text{ cm s}^{-1}} \right) \times \left( \frac{t_{\text{age}}}{1000 \text{ yrs}} \right). \quad (\text{A.18})$$

This equation is always satisfied since  $w_u$  and  $w_d$  range 0.01–0.1 pc and 0.06–0.4 pc, respectively.

Finally in order to validate Eqs. (A.8) and (A.9), we confirm the conditions

$$K_u / u_s < (K_u t_{\text{cool}})^{\frac{1}{2}}, \quad (\text{A.19})$$

$$u_d t_{\text{cool}} > (K_d t_{\text{cool}})^{\frac{1}{2}}, \quad (\text{A.20})$$

are always satisfied for the parameters of our interest. Using Eqs. (1), (6) and (10), Eq. (A.19) can be rewritten as

$$f < 19.0 \left( \frac{u_s}{2.89 \times 10^8 \text{ cm s}^{-1}} \right)^2 \left( \frac{\nu_{\text{rolloff}}}{2.6 \times 10^{17} \text{ Hz}} \right)^{-1}. \quad (\text{A.21})$$

This equation, together with Eq. (A.12), reduces

$$\frac{w_u}{w_d} < r, \quad (\text{A.22})$$

which is always satisfied since  $w_u = 0.01\text{--}0.1 \text{ pc}$  and  $w_d = 0.06\text{--}0.4 \text{ pc}$ . On the other hand, from Eqs. (1), (7), (10), and (A.20), we derive

$$g < 1.2 \left( \frac{r}{4} \right)^{-2} \left( \frac{u_s}{2.89 \times 10^8 \text{ cm s}^{-1}} \right)^2 \left( \frac{\nu_{\text{rolloff}}}{2.6 \times 10^{17} \text{ Hz}} \right)^{-1}. \quad (\text{A.23})$$

Combining this equation and Eq. (A.13), we eliminate  $\nu_{\text{rolloff}}$  and  $u_s$  as

$$\left[ 1 - \left( \frac{r}{4} \right)^{-1} \phi \right] g < \frac{1}{4} \left( \frac{r}{4} \right)^{-2} \phi R(\theta)^{-2} f. \quad (\text{A.24})$$

As long as  $r \leq 4$ , this is always satisfied since  $1 - (r/4)^{-1} \phi = (r-4)/(r-1) \leq 0$ .

## References

- Achterberg, A., Blandford, R.D., & Reynolds, S.P. 1994, A&A, 281, 220
- Aharonian, F.A., & Atoyan, A.M. 1999, A&A, 351, 330
- Allen, G.E., Petre, R., & Gotthelf, E.V. 2001, ApJ, 558, 739
- Bamba, A., Yamazaki, R., Ueno, M., & Koyama, K. 2003a, ApJ, 589, 827
- Bamba, A., Yamazaki, R., Ueno, M., & Koyama, K. 2003b, Adv. Space Res. in press (astro-ph/0308322)

Bell, A.R. 1978, MNRAS, 182, 443

Berezhko, E.G., Ksenofontov, & L.T. Völk, H.J. 2002, A&A, 395, 943

Berezhko, E.G., Ksenofontov, & L.T. Völk, H.J. 2003, in proceedings of 28th ICRC, p.2441

Blandford, R.D., & Eichler, D. 1987, Phys. Rep., 154, 1

Blandford, R.D., & Ostriker, J.P. 1978, ApJ, 221, L29

Drury, L.O'C. 1983, Rep. Prog. Phys., 46, 973

Dyer, K.K., Reynolds, S.P., Borkowski, K.J., Allen, G.E., & Petre, R. 2001, ApJ, 551, 439

Ellison, D.C., Berezhko, E.G., & Baring, M.G. 2000, ApJ, 540, 292

Ghavamian, P., Winkler, P.F., Raymond, J.C., & Long, K.S. 2002, ApJ, 572, 888

Jones, F.C., & Ellison, D.C. 1991, Space Science Rev., 58, 259

Jokipii, J.R. 1987, ApJ, 313, 842

Koyama, K., Petre, R., Gotthelf, E.V., Hwang, U., Matsura, M., Ozaki, M., & Holt S.S. 1995, Nature, 378, 255

Long, K.S., Reynolds, S.P., Raymond, J.C., Winkler, P.F., Dyer, K.K., & Petre, R. 2003, ApJ, 586, 1162

Lucek, S.G., & Bell, A.R. 2000, MNRAS, 314, 65

Malkov, E., & Drury, L.O'C. 2001, Rep. Prog. Phys., 64, 429

Ratkiewicz, R., Axford, W.I., & McKenzie, J.F. 1994, A&A, 291, 935

Reynolds, S.P. 1998, ApJ, 493, 375

Reynolds, S.P., & Keohane, J.W. 1999, ApJ, 525, 368

Skilling, J. 1975, MNRAS, 172, 557

Tanimori, T., Hayami, Y., Kamei, S., Dazeley, S.A., Edwards, P.G., Gunji, S., Hara, S., Hara, T. et al. 1998, ApJ, 497, L25

Tanimori, T., Naito, T., Yoshida, T., & CANGAROO collaboration 2001, to appear in proceedings of 27th ICRC, astro-ph/0108031

Vink, J., & Laming, J.M. 2003, ApJ, 584, 758

Völk, H.J., Berezhko, E.G., & Ksenofontov, L.T. 2003, A&A, 409, 563

Winkler, P.F., Gupta, G., & Long, K.S. 2003, ApJ, 585, 324